Bond-Angle-Potential-Dependent Dissipative Particle Dynamics Simulation and Lipid Inverted Phase

Da-Wei Li, X. Y. Liu,* and Y. P. Feng

Department of Physics, Faculty of Science, National University of Singapore, 2 Science Drive 3, Singapore 117542

Received: February 23, 2004; In Final Form: May 13, 2004

A bond-angle-potential-related dissipative particle dynamics (DPD) simulation method was established for the first time to simulate the inverted phase of a lipid. We observed that the correct elastic properties of the membrane in the DPD model can be reproduced by introducing a proper bond angle potential. Using this modified model, we succeed for the first time in producing spherical micellar, rodlike micellar, disklike micellar, and three types of inverted phases and phase sequences with different architecture. The results are in excellent agreement with the experiments and theory. The model can be applied for the simulation of biomembrane fusion and other dynamical processes associated with lipid phase behavior.

1. Introduction

The structures and properties of lipid bilayer membranes surrounding living cells are very relevant in many processes in organisms.[1] As a simplified model to the complexity of natural membranes, most researchers mainly focus on lipid membranes and lipid bilayer vesicles. In their studies, these membranes and vesicles are often composed of a single type of lipid, without embedded inclusions.[2,3] In these systems, dynamic processes occurring within a membrane involve cooperative changes over a distance much larger than the molecular size and a time scale much longer than the molecular vibrational periods.

To interpret the experimental results, the theoretical understanding of the dependence of membrane stability and material properties on the constituent lipid molecular structure and membrane composition is required. In tackling this issue, several groups have applied the mean-field approach[4−6] to explore the effects exerted on the chain organization, elastic modulus, stress profile, and stability of different lipid phases by variations on the head areas, tail lengths, and populations of lipid mixtures. Similarly, lattice-based Monte Carlo (MC) simulations have also been applied to study the evolution of microstructures in surfactant systems containing water and oil.[7] Nevertheless, both approaches have encountered some difficulties: the lattice-based simulations cannot capture the full Galilean invariance of a membrane, whereas the mean-field approach focuses on chain organization only and is incapable of handling the fluctuations within such a system. Apart from this, in most previous macroscopic theoretical studies on bilayer membranes and vesicles, the membranes are treated as smooth and continuous thin surfaces[8] (the so-called continuum models). Although many phenomena have been successfully described by these continuum models based on the bending energy and the frustration energy minimization, the molecular structures of lipids are not taken into account explicitly. This may cause problems on small scales. On the other hand, molecular dynamics (MD) simulations[9,10] are able to include more atomic details. Nevertheless, such simulations are restricted to small system sizes and short times. To overcome this problem, coarse-grained (CG) MD simulations have been used to extract the area compression modulus and bending modulus of single-component lipid bilayers and monolayers and their lateral stress distribution.[11] However, the application of MD simulations, including CG MD simulations, to the liquid biomembrane is restricted by current computational power to membrane patches that contain only a few hundred lipid molecules and the requisite solvent molecules. Because of these limitations, more CG models, such as the dynamical energy density function, Brownian dynamical (BD) simulation, and dissipative particle dynamic (DPD) simulation, have been derived.[12] Among these models, DPD has been proven to be a powerful method because it is an off-lattice, dynamical model with hydrodynamic interactions.[13−15]

Note that DPD simulation has been successfully applied to examine some of the behavior of lipid solutions[16−20] and amphiphile emulsion[21] phases. In a recent paper by Groot,[16] the DPD technique was applied with some success to simulate the appearance of pores in model lipid bilayers as a function of the concentration of a nonionic cosurfactant. The lipid phosphatidylethanolamine (PE) and surfactant $C_{12}E_6$ or C_9E_8 were used, and the parameters are extracted from the solubility data of the lipid and surfactant. The model is validated by the average area per molecule, the density profile, the stress profile, and the surface and bulk diffusion coefficients. It has been shown that the DPD model can produce a stress profile of biomembranes similar to that of the CG MD simulation, when the bond angle potential is added.[17] These two pieces of work show that the DPD model can describe the lipid bilayer phase and the biomembrane quite well. At the same time, the behavior of the micellar, hexagonal, lamellar, and L2 phases of short-tail amphiphiles obtained by the DPD model[18,19] were also reported.

Lipid inverted phases are very important in the formations of microsomes, mitochondria, tight junctions between cells, membrane fusion, and drug delivery. To the best of our knowledge, these phases have not been achieved yet using DPD simulation. If the DPD model is capable of describing the lipid solution system, it should be able to reproduce the phase behavior with different lipid architectures reasonably well under various conditions. In this paper, a modified DPD model is

* Author to whom correspondence should be addressed. E-mail: phyliuxy@nus.edu.sg.

10.1021/jp049180f CCC: $27.50
Published on Web 06/23/2004

presented to simulate the lipid inverted phase and produce the entire hypothetical phase diagram. This includes all phases from the micellar phase to the inverted micellar phase.[22] Note that such a complete phase diagram has never been simulated previously. More importantly, such a phase diagram is absolutely essential for the simulation of dynamic processes such as membrane rupture and fusion.

2. Modified DPD Model

2.1. Basic DPD Model. The basic DPD model described here is mainly based on the work by Groot and Warren.[15] The elementary units in a DPD simulation are fluid elements of soft beads. Beads interact via effective forces that are chosen to reproduce the hydrodynamic behavior of the fluid without reference to their molecular structure. The range of the force determines the size of the soft beads. In our model, there are three types of beads: water beads, hydrophilic head beads, and hydrophobic tail beads. All water and head beads have the same mass (m_0) and radius (r_0). These set the mass and length scale in the simulation. The time scale must be extracted from the dynamics of the relevant processes in the simulated fluid, such as diffusion. As suggested by Groot and Warren,[15] a value of $k_BT = 1$ was used in the simulation, which effectively specifies a unit of time. Unlike former models, the head beads that we will use have a radius that varies from $1r_0$ to $1.2r_0$ and the mass varies proportionally, according $m \propto r^3$.

There are three types of forces in the DPD model: (i) a conservative force that characterizes each pair of bead types uniquely and serves as a measure of hydrophobicity between hydrocarbon and water; (ii) a random force that creates relative momentum between bead pairs; and (iii) a dissipative force that destroys relative momentum.

The conservative force between two beads i and j, separated by a distance r_{ij}, is

$$F_{ij}^{c} = a_{ij}\left(1 - \frac{r_{ij}}{r_c}\right)\vec{r}_{ij} \qquad (1)$$

for $r_{ij} < r_c$ and is zero otherwise. The parameter r_c is defined as $r_c = (r_i + r_j)/2$, where r_i and r_j are the radii of beads i and j, respectively. The range of the force is characterized by r_c, and a_{ij} is the maximum repulsion between beads of types i and j. The parameter r_{ij} is the distance between the centers of the beads i and j, and $\vec{r}_{ij}$ is the unit vector pointing from bead j to bead i.

The dissipative force between two beads takes the form

$$F_{ij}^{D} = -\gamma_{ij}\left(1 - \frac{r_{ij}}{r_c}\right)^2(\vec{r}_{ij}\bullet\vec{V}_{ij})\vec{r}_{ij} \qquad (2)$$

for $r_{ij} < r_c$ and is zero otherwise, where γ_{ij} is the strength of the dissipation between beads i and j, and $\vec{V}_{ij} = \vec{V}_i - \vec{V}_j$ is their relative velocity.

Finally, the random force between a bead pair is

$$F_{ij}^{R} = \sqrt{2\gamma_{ij}k_BT}\left(1 - \frac{r_{ij}}{r_c}\right)\zeta_{ij}\vec{r}_{ij}\Delta t^{-1/2} \qquad (3)$$

for $r_{ij} < r_0$ and is zero otherwise. Values of the random force are generated by sampling a uniform random variable $\zeta_{ij}(t)$, that satisfies $\langle\zeta_{ij}(t)\rangle = 0$ and $\langle\zeta_{ij}(t)\zeta_{i'j'}(t')\rangle = (\delta_{ii'}\delta_{jj'} + \delta_{ij'}\delta_{ji'})\delta(t - t')$. Δt is the time step used in the simulation. The appearance of $\Delta t^{-1/2}$ is to ensure that the diffusion of particles is consistent, i.e., it is independent of the step size of the integration, as discussed by Groot and Warren.[15]

TABLE 1: Bead−Bead Conservative Force Parameters (a_{ij}), Dissipative Force Parameters (γ_{ij}), and Hookean Bond Potential Parameters (K, l_0) for All Bead Pairs

bead pair	a_{ij} (k_BT/r_0)	γ_{ij} ($\sqrt{m_0k_BT/r_0^2}$)	K (k_BT/r_0^2)	l_0 (r_0)
HH	25	4.5		
TT	25	4.5	128	0.5
WW	25	4.5		
HT	95	20	128	0.5
TW	95	20		
WH	25	4.5		

Water molecules are represented by discrete beads. Lipid molecules are represented by one head bead and several tail beads interconnected linearly together by a spring. The potential energy between the connected beads is $u_2 = {}^1/_2k(l - l_0)^2$, where l denotes the distance of the two beads.

The maximum repulsive force a_{ij} is chosen to be $25k_BT/r_0$ between two beads of the same type, and this coincides with the compressibility of water at room temperature.[15] In our simulation, the water−head, head−tail, and water−tail repulsive interactions are assumed to be equal to $25k_BT/r_0$, $95k_BT/r_0$, and $95k_BT/r_0$, respectively. Here, the quantity $95k_BT/r_0$ is large enough to create a phase separation between dissimilar beads. The bond stiffness (K) is taken as $128k_BT/r_0^2$ for a very stiff chain, and the bond length (l_0) is taken as $0.5r_0$. Table 1 summarizes all the bead−bead interaction parameters and the bond strength used in our simulation.

Julian and Lipowsky first introduced the concept of bond angle potential.[17] It is modeled by a three-body potential acting among adjacent bead triplets in the hydrocarbon tail chain: $u_3 = k_2[1 - \cos(\phi - \phi_0)]$, where ϕ is the bond angle of the two bonds connecting beads $(i - 1, i)$ and $(i, i + 1)$. A preferred angle of $\phi_0 = 0$ is used so that the potential minimum occurs for parallel bonds in a chain. The bond angle potential K_2 is $20k_BT$ at the tail in their model. It is zero when any bead is a head bead.

In all simulations, the time step is 0.05 DPD units. A modified Euler-type integration algorithm[15] is applied, where the parameter λ is set to 0.5. A self-developed program is used in our simulation. In a typical simulation box with 64 000 beads, a run of 10^4 steps requires ∼2 h in the HP workstation xw6000 with a 2.66 GHz XEON computer processing unit (CPU).

2.2. Choice of the Bond Angle Potential Parameter. As previously mentioned, the published DPD models succeed in reproducing the lipid micellar and lamellar phases, with various parameter sets.[16−20] These models have achieved some success in describing the properties of biomembranes.[16,17] However, inverted phases, such as the inverted bicontinuous phase, inverted hexagonal phase, and inverted cubic phase, have never been obtained by these models, despite their importance in biosystems. Our recent simulations show that these previous models are incapable of producing the lipid inverted hexagonal phase, which means that the aforementioned CG model is insufficient to simulate the hexagonal formation of the inverted phase.

To address this issue, we will focus on the DPD model. As a first step, we recall the CG process of this model. DPD was first introduced to simulate the fluid dynamics.[13,14] The elementary units in a DPD simulation are fluid elements of soft beads. The conserve force is used to reproduce the liquid $N-V$ equation.[13] The dissipative force and the random force worked as a thermometer. DPD model was later studied systematically and extended to polymers by Groot and Warren.[15] The density

of the beads and the repulsive force parameters between beads of same type come from the compressibility of water in room temperature. The repulsive parameters between different types of beads were deduced from the Flory−Huggins theory. Note that, in the DPD modeling, the CG process from the atomistic models is a conceptual step, rather than a well-defined quantitative procedure. It relies on the observation that a variety of real physical systems with very different microscopic interactions share the same qualitative behavior on a mesoscopic scale. In this regard, most DPD simulations use a conceptual repulsive parameter set rather than real molecules. The bond angle potential was simply discarded in the aforementioned CG process. Such potentials were determined to be unnecessary in obtaining polymer microphase separation. However, as a drawback, chain-flexibility-related parameters are excluded in the aforementioned approach. The bond angle potential in DPD model eventually decides the chain flexibility. In this sense, the proper bond angle potential should be included, to analyze the elastic property of a bilayer-based membrane.

As the first step, a correct DPD model must be able to reproduce the correct area stretch behavior and tension profile of a known system, at least qualitatively. The area stretch modulus and tension profile have been obtained using full atomic MD simulation[23] and the CG molecular model.[11,24] The two models exhibit similar qualitative results. The DPD models without a bond angle potential also have achieved similar results.[16] Julian and Lipowsky[17] showed that a DPD model with a bond angle potential of $20k_BT$ can produce a more accurate tension profile, resulting in two positive peaks in the tail region. However, the stretch modulus increases and the area per molecule decreases when the tail length increases if the bond angle potential is $20k_BT$. This unfortunately disagrees with the experiments.[25] Therefore, the bond angle potential should be not too large. When it is small, such as $5k_BT$, the area stretch modulus is independent of the tail length and the area per molecule increases when tail becomes longer. These results agree well with the experiments.[25]

Second, a correct CG model should be able to reproduce the response of the tension profile, with respect to different deformation. Note that this issue has never been studied previously by any CG model. The tension profile and its derivation eventually dominates the spontaneous curvature of the monolayer, the area stretch modulus, the bending modulus, and the Gauss bending modulus of the bilayer.[4−6,8] We examine the tension profile and its derivation with area stretch deformation in a DPD model. A lipid model with one headgroup and nine tail beads is used. The solid and dotted curves in Figure 1a show the tension profiles across a bilayer in a tensionless state and a small tension state (the area is enlarged by 7%), respectively. The bond angle potential is zero; other parameters are listed in Table 1. When the bond angle potential is $5k_BT$, the tension profile in a tensionless state and a small tension state (the area is enlarged by 7%) is shown in Figure 1b.[26]

The *x*-axis in Figure 1 is the relative position of the slice. A value of zero corresponds to the midplane of the bilayer. The high positive peak corresponds to the hydrocarbon tail/water interface. The *y*-axis is the tension/thickness in this slice (k_BT/r_0^3). As shown in Figure 1, although DPD models with different bond angle potentials show similar tension profiles, they reveal different tension profile responses, with respect to the stretch deformation. If the bond angle potential is zero, the tension in the interfacial region changes significantly, whereas the tension in the hydrocarbon tail region (the slice from −40 to 40) exhibits little change when the area is stretched. This

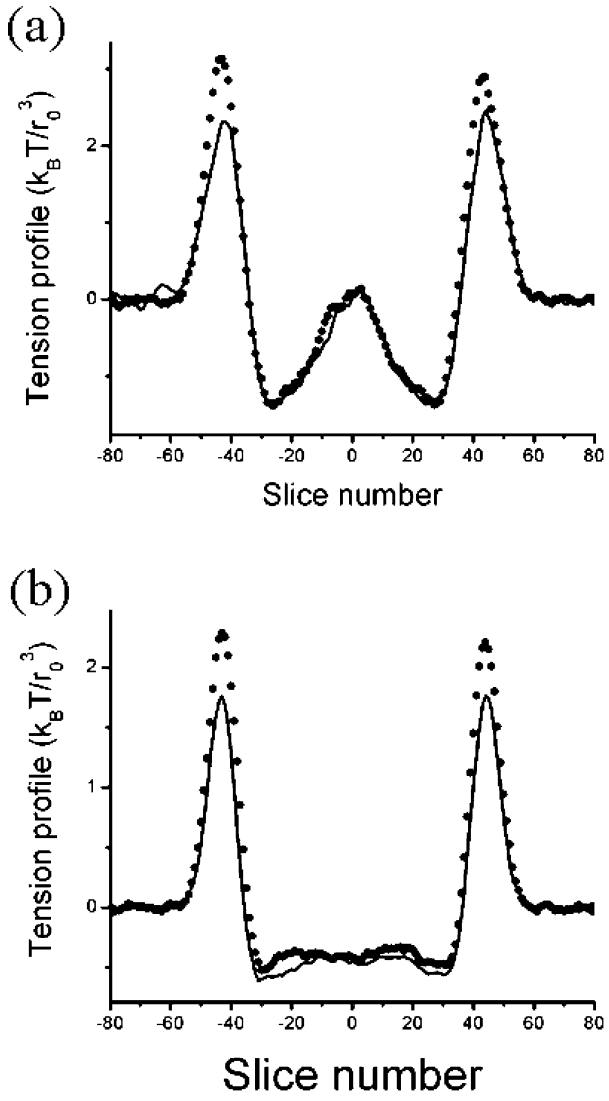

Figure 1. 1. Tension profile and its change with respect to stretch; the solid curve is the tension profile in a tensionless state, whereas the dotted curve is in a tension state (for bond angle potentials of (a) 0 and (b) $5k_BT$). (Area is enlarged by 7%.) The x-axis represents the slice position. Zero corresponds to the midplane of the bilayer. The positive peaks correspond to the water/hydrocarbon interface.

means only the interfacial region contributes to the area stretch modulus of the bilayer. When a moderate bond angle potential of $5k_BT$ is chosen, the tension also changed remarkably in the tail region. Unfortunately, it cannot be decided which one is better, a direct comparison with full atomic MD simulation or experiments, which have not been reported yet. However, some useful information from CG MD simulation and experiments can be used to examine this point.

In a CG MD simulation,[11] the bending modulus is related to the area stretch modulus by

$$K_{\text{bend}} = \frac{K_A h^2}{48} \tag{4}$$

where K_{bend} is the membrane bending modulus, K_A the area stretch modulus, and h the thickness of the membrane. This expression is based on the idea that the membrane can be seen as a thin solidlike film with vanishing shear modulus, which has been approved by experiment to be correct quantitively.[25] The more precise formula should be[25]

$$K_{\text{bend}} = \frac{K_A(h - h_0)^2}{24} \quad (5)$$

where h_0 is a coefficient that is decided by the headgroup and is independent of the tail length. If only the interfacial region in the bilayer contributes to the membrane area stretch modulus, as in the case of a DPD model with zero bond angle potential, the h term in eq 4 should be replaced by the thickness of the interfacial region. This means that the bending modulus will be too small in such a membrane model. Our simulations have indicated that a membrane with zero bond angle potential is much easier to bend when it is compressed. Similarly, the too-small bending modulus may be attributing to the failure of such models in reproducing the inverted hexagonal phase. Nevertheless, it is still capable of producing an inverted rodlike phase, where the radius of the rod has a wide distribution. In a DPD model with a bond angle potential of $5k_BT$, the entire region of the bilayer will contribute to the area stretch modulus. This means that the relationship between the area stretch modulus and the bending modulus will be satisfied approximately. Note that the necessity of a bond angle potential to make a correct CG model only exists in the DPD model, whereas it is irrelevant in the CG MD model. This difference may come from the soft repulsive force without a hard core that is used in the DPD model, as discussed by Julian and Lipowsky.[17]

Note that we reach this conclusion by analyzing the elastic response of the different parts of the modeled membranes rather than performing a well-defined quantitative procedure, which seems hopeless for the DPD model, because of its conceptual CG nature. The tension profile and its response to the stretch of a real lipid membrane are impossible to obtain experimentally. They have been obtained by means of a polymer brush model,[25] a mean-field model,[5,6] and CG MD simulations.[11,24] The DPD model with a small-angle bond potential introduced in this section should also be a good approximation for lipid molecules in a liquid crystal phase, because it creates a reasonable relationship between the area stretch modulus and the bend modulus of the membrane. This means that the bond angle potential is necessary for a DPD model to describe the conformation and the tension of the hydrocarbon chains correctly. Although such a model is used to examine the elastic property of the membranes, it is also applicable in all liquid crystal phases, including the inverted hexagonal phase.

Note that the choice of the bond angle potential should be dependent on the other parameters used, such as the repulsive parameters, and will be different from lipid to lipid. The key problem is that, as a conceptual CG model, the bond angle potential should be selected to reproduce correct phase behavior of the lipids. In this regard, the DPD model has been successful in reproducing the phase sequence of lipids with different head sizes and tail lengths when the bond angle potential is set to $5k_BT$, using the parameters listed in Table 1.

3. Verification of the Bond-Angle-Dependent DPD Model

The validation of the average area per lipid, the density profile, and the surface and bulk diffusion coefficients can be achieved easily in most DPD simulations; therefore, that validation will not be performed here. We will, in the following, focus on the verification on the phase behavior of the modeled lipids. Notice that, in some DPD simulations, the simulation parameters were extracted from real lipids using the Flory−Huggins theory,[16] whereas in others case, arbitrary parameters were chosen without a direct link to real lipids.[17−20,27,28] In the first case, it is important to validate the model by confirming that the simplified lipids will still give the correct phase, and, in the latter case, we must use a model with a designed phase behavior. In this concern, verification on the phase behavior is essential for a correct DPD model.

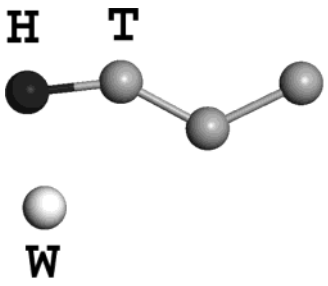

Figure 2. 2. Depiction of one HT3 lipid molecule and one water molecule; the head, tail, and water beads are represented by dark, gray, and white balls, respectively. Lipids are modeled by one head bead and several tail beads, connected together by springs.

TABLE 2: Typical Phases for Amphiphilic Molecules with Different Architectures[a]

head size	HT1	HT2	HT4	HT6	HT10	HT12
1.2	sphere	disk	disk	bicon	bicon	bicon
1.1	rod	disk	bicon	bicon	H_{ii}	H_{ii}
1.0	rod	disk	H_{ii}	H_{ii}	M_{ii}	M_{ii}

[a] Legend is as follows: sphere, spherical micellar phase; rod, rodlike micellar phase; disk, disklike micellar phase; bicon, inverted bicontinuous phase; H_{ii}, inverted hexagonal phase; and M_{ii}, inverted micellar phase.

The phase behavior of lipid molecules with different tail chain lengths and head sizes will be examined to validate the model here. For such molecules, the nomenclature "HTN (a)" means a molecule of one head bead and N tail beads. The size of the head beads are a times r_0. As an example, one HT3 (1.0) molecule and one water molecule are depicted in Figure 2, where the dark ball represents the head, the gray balls represent the tail, and white balls represent water beads. This scheme will be adopted throughout this work except in Figures 4 and 7. Water beads are suppressed from the view for the sake of clarity, where appropriate.

Simulations are performed within a cubic box with a constant volume of $V = L^3$. (L is the simulation box side length.) Periodic boundary conditions are applied in all three dimensions to eliminate edge effects. The simulation box is filled with beads of the chosen density $\rho = 3m_0/r_0^3$, which represents the mass-to-volume ratio of the box. The concentration of amphiphilic molecules, which is defined as the ratio of the number of amphiphilic beads to the total number of beads, will be given below. In the initial state, the molecule positions are assigned randomly. The bead momenta are assigned from a Maxwell distribution of which the temperature is 1 DPD unit. Unless specified, the simulation box contains 8000 beads for HT1 and HT2, 27 000 beads for HT3 and HT4, and 64 000 beads for HT10 and HT12.

In our simulations, micellar, hexagonal, lamellar, inverted bicontinuous phases, as well as inverted hexagonal and inverted micellar phases, are identified when the concentration, tail length, and head size are allowed to vary. The phase behavior, as a function of head size and tail length, is summarized in Table 2. The terms "sphere" and "rod" denote spherical micellar and rodlike micellar phases, respectively. The term "disk" denotes a disklike micellar phase. The term "bicon" denotes the inverted bicontinuous phase. The term "H_{ii}" denotes the inverted hexagonal phase, and the term "M_{ii}" denotes the inverted micellar phase. The effect of concentration is given in

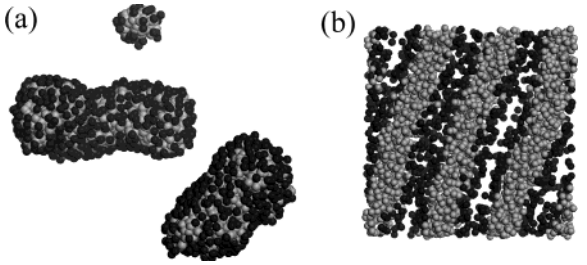

Figure 3. (a) Phase formation of HT2 (1.0); the concentration is 6%, and the time is 2200 DPD units. Water is suppressed from the figure, for the sake of clarity. Two rodlike vesicles and one micelle remain in the simulation box. (b) Phase formation of HT2 (1.2); the concentration is 80%, and the simulation time is 2500 DPD units. Water is suppressed from the figure, for the sake of clarity. A lamellar phase forms, and the bilayer is reorientated in a special way to maintain the period.

the text separately. As shown in Table 2, all phases obtained can be divided into two regimes: the normal phases (lipids formation in water) and the inverted phases (water formation in lipids). In this work, we only focus on the inverted phase.

3.1. Formation of the Normal Phase. When the tail length is short, such as HT1, the amphiphilic molecules will aggregate rapidly into spherical or rodlike micelles, because these molecules have a strong tendency to segregate from water and bend toward the tail. As the concentration increases, the interaction between different micelles cannot be neglected. This causes the formation of a hexagonal phase and a lamellar phase. This result is consistent with that reported by Prinsen[19] using a similar DPD model.

As the tail becomes longer, such as HT2, spherical or rodlike micelles are no longer stable, and the disk-shaped micelles prevails as the most stable phase. Vesicles will form spontaneously in some cases, to eliminate the edge free energy. This occurs, in particular, when the concentration is not very high. On the other hand, if the interaction between the different micelles cannot be neglected, the bending of the bilayers will be suppressed. As a consequence, the lamellar phase will form. Spontaneous formation of vesicles has been reported using the amphiphile HT4 at low concentration and a low temperature equal to 0.43 DPD units.[27,28] We obtained a similar result using HT2 (1.0) at a temperature of 1 DPD unit and a concentration of 6%. In this run, finally, only two large rodlike vesicles and one small micelle remain, as shown in Figure 3a. The simulation time was 2200 (in DPD units). In this figure, to gain a better view, the water beads are suppressed. The other amphiphilic molecules (HT2 (1.1), HT2 (1.2) and HT4 (1.2)) give a similar result. We have also tested HT2 (1.2) at a high concentration (80%) and a lamellar phase forms within a time period of 2500 DPD units, as shown in Figure 3b. In this image, water beads are suppressed.

3.2. Formation of the Inverted Phase. When the chain length is long and the head size is not too large, the lipids have a tendency to curve toward the head. This results in the formation of three types of inverted phases. The phases are the inverted bicontinuous phase for HT4 (1.1), HT6 (1.1), HT6 (1.2), HT10 (1.2), and HT12 (1.2), the inverted hexagonal phase for HT10 (1.1), HT12 (1.1), HT4 (1.0), and HT6 (1.0), and the inverted spheral micellar phase for HT10 (1.0) and HT12 (1.0).

For all these aforementioned inverted phases, no phase transition is observed when the concentration becomes very low, but a phase separation emerges instead. Here, HT4 (1.0) is chosen as an example. (HT4 (1.0) will exhibit an inverted hexagonal phase, which will be discussed in detail below.) Figure 4a, b, and c shows the formation of HT4 (1.0) at

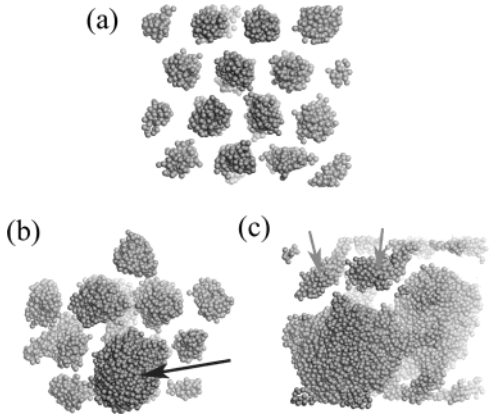

Figure 4. Phase formation of HT4 (1.0) at different concentrations. Only water beads are shown here. (a) Concentration is 80%, and a regular inverted hexagonal phase form (total simulation time is 50 000 DPD time units). (b) Concentration is 70%, and a large water aggregation, marked by the dark arrow is formed, whereas the other parts of the simulation box exhibit an inverted hexagonal-phase-like formation (total simulation time is 100 000 DPD time units). (c) Concentration is 65%; two big water balls are formed and only several water rods can be identified in the remaining region, marked by the gray arrows (total simulation time is 50 000 DPD time units).

concentrations of 80%, 70%, and 65%, respectively. The total simulation times require 50 000, 100 000, and 50 000 DPD units of time, respectively. Only water beads are shown, whereas the head beads, which surround the water rod, and the tail beads, which fill the remaining region, are suppressed. In Figure 4a, the water beads form rods and the different rods pack into a hexagonal structure. The figure is viewed along the water rod direction. No phase separation can be identified. On the other hand, in Figure 4b, when the concentration is low, a large aggregate of water beads forms, marked by the dark arrow in the figure. At the same time, water and amphiphilic molecules form an inverted hexagonal phase in the remaining domain, apart from the fact that the formation of this region rich in lipids shows a high degree of disorder. Such a result is due to the finite size effect: our simulation box is not sufficiently large; therefore, the interface between the two phases is much too large, compared to the total volume of the two phase regions. This interface will disturb the ordered domain. Similarly, the water aggregation exhibits an approximately rodlike shape. In Figure 4c, the concentration of lipids is reduced further and two big water balls, representing an aqueous lipid solution phase, occupy most of the space. At the same time, several rodlike water channels, marked by the gray arrows in the figure, are still discernible. These correspond to a phase that is rich in lipids. Compared to Figure 4b, the aqueous solution region becomes larger and the lipids-rich region becomes smaller. Although the finite size effect is pronounced here, a low concentration obviously will induce a phase separation for these long-tail amphiphilic molecules. Note that we focus on the appreciable phase relationship of different lipids with different structures. In the sequel, we show only the simulated phase at some discrete value of the concentrations without any phase separation.

The phases formed by HT12 (1.0) with water are shown in Figure 5. This is an example of an inverted micellar phase. The total simulation time is 75 000 DPD units. The concentration of HT12 (1.0) is 90%. Figure 5a shows only one cross section of the entire simulation box. Figure 5b shows the cross section of a ball of water molecules and the surrounding amphiphilic molecules in detail. Water beads are suppressed in Figure 5b. As shown in Figure 5, water beads form spheres and have a random spatial distribution, being surrounded by head beads,

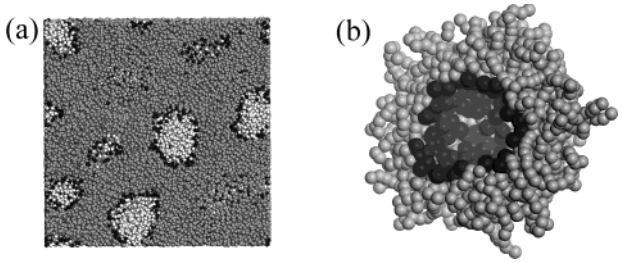

Figure 5. Phase formation of HT12 (1.0); the concentration is 90%, and the total simulation time is 75 000 DPD units. (a) The cross section of the entire simulation box: discrete water balls distribute randomly and amphiphilic molecules fill the remaining region. (b) Cross section of one ball of water and its surrounding amphiphilic molecules; water is suppressed from the figure, for the sake of clarity.

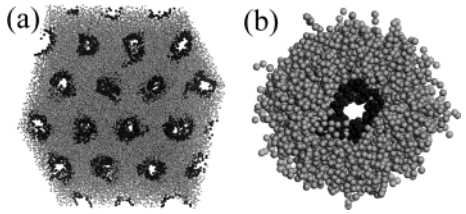

Figure 6. 6. Phase formation of HT10 (1.1); the concentration is 90%, and the simulation time is 75 000 DPD units. (a) The entire simulation box: water rods stalk into a 2-D 6-fold structure. (b) One rod and its surrounding amphiphilic molecules: the terminal tail beads form a hexagonal shape, whereas the hydrophilic/hydrophobic interface does not show any stable shape. Water is suppressed from the figure, for the sake of clarity.

whereas the tail beads fill the remaining region. No cubic symmetry can be observed. Therefore, it is an inverted micellar phase.

The phases formed by HT10 (1.1) are shown in Figure 6. This is an example of an inverted hexagonal phase. The total simulation time is 75 000 DPD units. The concentration of HT10 (1.1) is 80%. Figure 6a shows the entire simulation box viewed along the rod direction. The water core, which is surrounded by head beads, forms rods and a stalk in a two-dimensional (2-D) 6-fold formation, and the tail beads fill the remaining region. One water core and the surrounding molecules are shown in Figure 6b in detail. The terminal tail beads have an approximately hexagonal shape, which is consistent with most of the models. The hydrophilic/hydrophobic interface is supposed to be round in most elastic models, and some works suggest that it is not a perfect circle but hexagonal instead. Nevertheless, we find that the fluctuation is too high to identify any stable shape.

The phases formed by HT6 (1.1) are shown in Figure 7. This is an example of an inverted bicontinuous phase. Only water beads are shown in Figure 7. The concentration of HT6 (1.2) is 80%. The total simulation time is 20 000 DPD units. Similar to the inverted hexagonal phase, water beads also form rods here. However, the rods have divergent structures and are interwoven with each other. In experiments, in total, three liquid crystal phases have been identified in this region, having the space groups *Ia*3*d* (Q^{220}), *Pn*3*m* (Q^{224}), and *Im*3*m* (Q^{229}). The structures consist of two sets of interwoven networks of water channels, separated by the gyroid and the F- and P-minimal surfaces. The detailed arrangements of the water channels are different. The phases obtained in our simulation also have two interwoven networks of water channels but show some randomness in the connection of the water channels and have no cubic symmetry. Therefore, it is only an inverted bicontinuous phase but not a bicontinuous cubic phase.

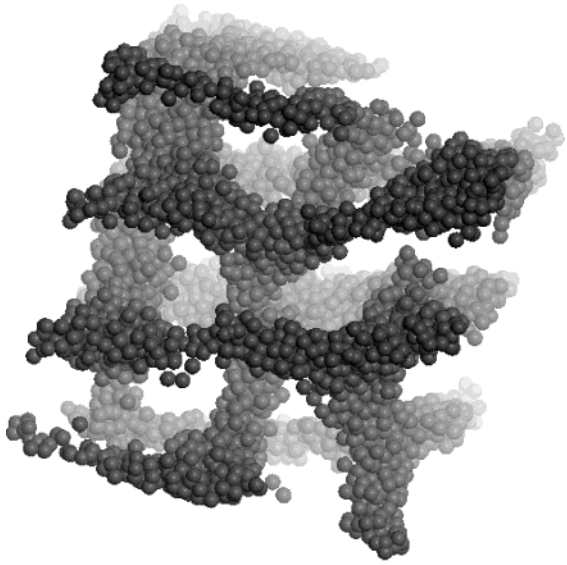

Figure 7. Phase behavior of HT6 (1.2); the concentration is 80%, and the simulation time is 2000 DPD units. Only water is shown; the entire structure consists of an interwoven network of water channels.

In regard to the identification of the phases, two facts must receive attention. First, an exact cubic structure cannot be expected unless the edge length of the simulation box (artificial period) is exactly equal to an integral multiple of the period of the cubic liquid crystal phase. In the simulation, for long-tailed lipids, we obtain only a random inverted micellar phase, whereas in the experiments, the space group *Fd*3*m* (Q^{227}) is the only inverted cubic phase that has been identified. Apart from this, one of the inverted bicontinuous phases in our simulation turns out to be a pseudo-bicontinuous cubic phase, which also has two interwoven networks of water channels but does not have cubic symmetry. In either case, it is impossible to conclude whether cubic symmetry is actually absent, or whether it is present but nonetheless suppressed because of the incompatibility between the period of the liquid crystal phase, on one hand, and the artificial introduced period, on the other hand. In fact, this effect also exists in the inverted hexagonal phase and the lamellar phase. All water rods or bilayers are reorientated in such a way to achieve a best fit between the artificial period and the period of the liquid crystal phase, as shown in Figures 3 and 6a. (Note that all simulation boxes are cubic.) In a three-dimensional (3-D) simulation box, the fit always can be achieved for a one-dimensional (1-D) or 2-D liquid structure. However, for a 3-D liquid crystal, this incompatibility becomes critical and it will disrupt the 3-D liquid crystal structure. This effect has also been discussed in the DPD simulation of the polymer blend.[29]

Second, the bilayer formation must be handed with care. When the initial concentration is not very high, lipids with a long tail will aggregate into bilayer structures rapidly at the beginning, because of the fact that the bilayer formation can minimize the dissimilar tail−water interaction. However, for the lipids that favor the inverted phase, the bilayer formation is, in fact, a metastable intermediate structure. After two bilayers approach and adhere to each other, they will then transform to complex structures of inverted rods or inverted micelles. This process requires a long simulation time. More importantly, if there is only one bilayer aggregate in the simulation box, it will be stable, even if the lipids favor the inverted nonlamellar phase. This may lead to the misinterpretation of the properties of the lipids. This is an important but commonly neglected point.

3.3. Comparison with Theory and Experiment. The phase behavior of amphiphilic molecules with variable tail lengths and head sizes agrees quite well with the experiment and theory.[22] It is well-known that increasing the lipid chain length or the number of chains per polar headgroup will strengthen the chain−chain interactions. This favors the formation of inverted nonlamellar phases. Any structures that increase the hydration of the phases will prevent the appearance of inverted nonlamellar phases, because it increases the head size and the pressure in the head region. Our simulation result agrees with this. The phase sequence from the spherical micellar phase to the rodlike micellar phase to the disklike micellar phase and to the inverted nonlamellar phase with different spontaneous curvature is well-understood.[22] However, the understanding of the different inverted phases is much more limited, because of the complex frustration energy exiting in the inverted phase. To the best of our knowledge, only several simple models[30−32] have been published. To summarize, when the spontaneous curvature changes from a small negative value to the most negative value (this means that the tail becomes longer or the head becomes smaller), the phase will tend toward the inverted bicontinuous phase, inverted hexagonal phase, and inverted micellar phase.[30−32] Our simulation result agrees with these two phase sequences quite well. Note that, for the inverted bicontinuous phase and the inverted micellar phase, no cubic symmetry can be identified, although different types of cubic phases have been observed in the experiments. This may come from the finite size effect, as discussed previously.

The effects of concentration shown in our simulation also agree with the experiments and theory. When the lipids favor the spherical or rodlike micellar phase, the interaction between different micelles will raise the free energy of the system when the concentration is relatively high. As a consequence, the hexagonal phase or the lamellar phase will occur. The aforementioned simulation result is consistent with this and the DPD simulation by Prinsen.[19] When the lipids favor the bilayer formation, a low concentration will produce a disklike micellar phase or sometimes a vesicle phase and a high concentration will result in the lamellar phase. Our simulation result also agrees with this. When the lipids favor the inverted nonlamellar phase, liquid−liquid phase separation will occur in most cases when the concentration become very low, which will give the formation of one lipid monomer solution phase and one lipids-rich phase will form.[22] However, in some cases, the addition of water may induce a phase transition due to the hydration and other effects.[33] We have observed the phase separation in our simulations for these lipids. We suggest that the phase transition induced by concentration may be observed if the parameters are tuned carefully. Note that the DPD model does not incorporate the hydration effect. This means that it cannot simulate phase transition via this effect.

4. Applications

The continuum model,[33] Monte Carlo (MC) simulations,[7] and the DPD model are all able to reproduce the lipid phase behavior. However, the DPD applied in this work has some particular advantages, especially in the simulation of the dynamic process of amphiphilic systems, such as membrane fusion. First, the DPD can server as a CG molecular mode, to describe the evolving process in the scale of membrane thickness and evaluations in lipid conformations. In contrast, these results cannot be obtained in the continuum elastic model. Apart from this, DPD model can provide direct information about the structure of the "void" in the inverted phase and fusion intermediate. Second, in comparison with lattice MC simulations, the DPD model preserves the full Galilean invariance of fluid. It has been suggested that hydrodynamic interactions can strongly affect the kinetics of domain growth in a polymer blend.[34] These effects on the process of membrane fusion and other collective membrane reorganization remain an open question. Hydrodynamic interaction has an important role in the DPD model, which is lacking in other CG models, including MC models and BD models. Third, an inverted hexagonal phase has been achieved by the CG MD model[35] and even a diamond phase has been achieved by full atomic MD simulation.[36] The MD method suffers from the small simulation cell and long CPU time. On the other hand, the DPD method described in this paper is able to adopt a large simulation box; therefore, the finite size effects can be minimized. Finally, the DPD model runs very fast, which allow us to parametrize the simulation to obtain the spontaneous curvature of lipids and study them systematically. Note that the time step in DPD simulation is much larger than that in a MD simulation, because of the repulsion without a hard core.

We should notice that, in the field of membranes science, special attention has been focused on membrane fusion for a long time. In this field, the so-called stalk model,[37] based upon continuum elastic calculation, is the generally accepted model and widely used. Continuum models treat the lipid membrane as a homogeneous elastic surface. The view that elastic models may be appropriate for describing the stalk model is mainly supported by the fact that they also provide a semiquantitative description of the inverted hexagonal phase. However, there are still differences in the structures between the inverted hexagonal phase and the fusion intermediate. The continuum models are dependent very much on the assumption of fusion pathways. In this concern, the fusion intermediate stage that has been tested may not be realistic. In contrast, the DPD model can overcome this difficulty. Applying the DPD approach developed in this work, we have successfully obtained the membrane's fusion pathway. The detailed result will be presented separately. Note that the DPD model has more applications, because of its high efficiency. The effect of segregation of mixing of lipids and amphiphilic peptide can be easily incorporated in this model and examined. Such a simulation is difficult to handle in the continuum elastic model.

5. Summary and Conclusions

The dissipative particle dynamics (DPD) technique has been modified to model the phase behavior of a lipid solution. First, by analyzing the tension response of a membrane with stretch deformation, we found that a proper bond angle potential should be included in the model, to describe the chain organization correctly. Second, based on a proper bond angle potential ($5k_BT$), various phases (in particular, the inverted phase of the amphiphilic molecule solution) are simulated by the DPD model. The occurrence of the phases with different architectures in different concentration regions agrees well with the experiment and theory. The system exhibits a spherical micellar phase, a rodlike micellar phase, a disklike micellar phase, an inverted bicontinuous phase, an inverted hexagonal phase, and an inverted micellar phase as the tails of the lipid molecules become longer or the heads become smaller. For lipids that favor the micellar phase, a high concentration of lipids in water can induce a phase transition to the hexagonal or lamellar phase; for lipids that favor the inverted phase, a lower concentration can induce a phase separation, which results in one amphiphile monomer solution phase and one amphiphile-rich phase. These mean that

the DPD model is fully capable of capturing the essential phase behavior of the amphiphilic system, despite the introduction of many approximations. Third, the DPD method can adopt a large simulation box to minimize the finite size effects and run very fast, in comparison with molecular dynamics (MD) simulations. Henceforth, this model is very suitable for studying dynamic phase behavior. The detailed phase diagram obtained in this work is also helpful to the dynamical simulations in biomembranes and other amphiphilic systems.

Acknowledgment. The authors are very much indebted to Dr. C. Strom for her valuable suggestions and proofreading of the manuscript. The research is supported by the Science & Engineering Research Council, Singapore (Project No. 0221010036).

References and Notes

(1) Lipowsky, R.; Sackmann, E., Eds. *Structure and Dynamics of Membranes, Handbook of Biological Physics, Vol. 1*; Elsevier Science: Amsterdam, 1995.

(2) Discher, B. M.; Hammer, D. A.; Bates, F. S.; Discher, D. E. *Curr. Opin. Colloid Interface Sci.* **2000**, *5*, 125.

(3) Seifert, U.; Lipowsky, R. In *Structure and Dynamics of Membranes, Handbook of Biological Physics, Vol. 1*; Lipowsky, R.; Sackmann, E., Eds.; Elsevier Science: Amsterdam, 1995.

(4) Ben-Shaul, A.; Szleifer, I.; Gelbart, W. M. *J. Chem. Phys.* **1985**, *83*, 3597.

(5) Szleifer, I.; Kramer, D.; Ben-Shaul, A.; Roux, D.; Gelbart, W. M. *Phys. Rev. Lett.* **1988**, *60*, 1966.

(6) Szleifer, I.; Kramer, D.; Ben-Shaul, A.; Gelbart, W. M.; Safran, S. A. *J. Chem. Phys.* **1990**, *92*, 6800.

(7) Larson, R. G. *J. Phys. II* **1996**, *6*, 1441.

(8) Helfrich, W. In *Physics of Defects*; Balian, R., Kléman, M., Poirier, J.-P., Eds.; North-Holland: Amsterdam, 1981.

(9) Scott, H. L. *Curr. Opin. Struct. Biol.* **2002**, *12*, 495.

(10) Saiz, L.; Klein, M. L. *Acc. Chem. Res.* **2002**, *35*, 482.

(11) Goetz Gompper, R. G.; Lipowsky, R. *Phys. Rev. Lett.* **1999**, *82*, 221.

(12) Shelley, J. C.; Shelley, M. Y. *Curr. Opin. Colloid Interface Sci.* **2000**, *5*, 101.

(13) Hoogerbrugge, P. J.; Koelman, J. M. V. A. *Europhys. Lett.* **1992**, *19*, 155.

(14) Espanol, P.; Warren, P. B. *Europhys. Lett.* **1995**, *30*, 191.

(15) Groot, R. D.; Warren, P. B. *J. Chem. Phys.* **1997**, *107*, 4423.

(16) Groot, R. D.; Rabone, K. L. *Biophys. J.* **2001**, *81*, 725.

(17) Shillcocka, J. C.; Lipowsky, R. *J. Chem. Phys.* **2002**, *117*, 5048.

(18) Jury, S.; Bladon, P.; Cates, M.; Krishna, S.; Hagen, M.; Ruddock, N.; Warren, P. *Phys. Chem. Chem. Phys.* **1999**, *1*, 2051.

(19) Prinsen, P.; Warren, P. B.; Michels, M. A. J. *Phys. Rev. Lett.* **2002**, *89*, 148302.

(20) Kranenburg, M.; Venturoli, M.; Smit, B. *J. Phys. Chem. B* **2003**, *107*, 11491.

(21) Rekvig, L.; Kranenburg, M.; Hafskjold, B.; Smit, B. *Euorphys. Lett.* **2003**, *63*, 902.

(22) Seddon, J. M.; Templer, R. H. In *Structure and Dynamics of Membranes, Handbook of Biological Physics, Vol. 1*; Lipowsky, R.; Sackmann, E., Eds.; Elsevier Science: Amsterdam, 1995.

(23) Lindahl, E.; Edholma, O. *J. Chem. Phys.* **2000**, *113*, 3882.

(24) Goetz Gompper, R. G.; Lipowsky, R. *J. Chem. Phys.* **1998**, *108*, 7397.

(25) Rawicz, W.; Olbrich, K. C.; McIntosh, T.; Needham, D.; Evans, E. *Biophys. J.* **2000**, *79*, 328.

(26) To obtain these, one bilayer was placed perpendicular to the *z*-axis. First, the average area per molecule is adjusted to obtain a tensionless bilayer. Next, the area is fixed to obtain the tension profile at the tensionless state. The area per molecule then is enlarged by 7% and the tension profile in this state is calculated. The calculation of the stress tensor for a system composed of point particles interacting via continuous potentials is described in ref 24. In this method, the contributions to the tension profile of the bead−bead interactions, bond stretching, and chain stiffness potentials are averaged over thin slices parallel to the bilayer surface. In our study, the simulation box is divided into 300 slices parallel to the bilayer surface.

(27) Yamamoto, S.; Maruyama, Y.; Hyodo, S. *J. Chem. Phys.* **2002**, *116*, 5842.

(28) Yamamoto, S.; Maruyama, Y.; Hyodo, S. *J. Chem. Phys.* **2002**, *117*, 2990.

(29) Groot, R. D.; Madden, T. J. *J. Chem. Phys.* **1998**, *108*, 8713.

(30) Hamm, M.; Kozlova, M. M. *Eur. Phys. J. E* **2000**, *3*, 323.

(31) Hamm, M.; Kozlova, M. M. *Eur. Phys. J. B* **1998**, *6*, 519.

(32) Duesing, P. M.; Templer, R. H.; Seddon, J. M. *Langmuir* **1997**, *13*, 351.

(33) Kozlov, M. M.; Leikin, S.; Rand, R. P. *Biophys. J.* **1994**, *67*, 1603.

(34) Groot, R. D.; Madden, T. J.; Tildesley, D. J. *J. Chem. Phys.* **1999**, *110*, 9739.

(35) Shelley, J. C.; Shelley, M. Y.; Reeder, R. C.; Bandyopadhyay, S.; Moore, P. B.; Klein, M. L. *J. Phys. Chem. B* **2001**, *105*, 9785.

(36) Marrink, S.; Tieleman, D. P. *J. Am. Chem. Soc.* **2001**, *123*, 12383.

(37) Siegel, D. P. *Biophys. J.* **1999**, *76*, 291.